INTERNATIONAL JOURNAL OF ROBUST AND NONLINEAR CONTROL
Int. J. Robust. Nonlinear Control 2010; **00**:1–17
Published online in Wiley InterScience (www.interscience.wiley.com). DOI: 10.1002/rnc

Computation of lower bounds for the induced $\mathcal{L}_2$ norm of LPV systems

Tamas Peni[1]* and Peter J. Seiler[2]

[1] *Systems and Control Laboratory of Institute for Computer Science and Control, 1111 Budapest, Kende u. 13-17., Hungary*
[2] *Aerospace Engineering and Mechanics Department, University of Minnesota, 107 Akerman Hall, 110 Union St SE, Minneapolis, MN 55455-0153*

SUMMARY

Determining the induced $\mathcal{L}_2$ norm of a linear, parameter-varying (LPV) system is an integral part of many analysis and robust control design procedures. Most prior work has focused on efficiently computing upper bounds for the induced $\mathcal{L}_2$ norm. The conditions for upper bounds are typically based on scaled small-gain theorems with dynamic multipliers or dissipation inequalities with parameter dependent Lyapunov functions. This paper presents a complementary algorithm to compute lower bounds for the induced $\mathcal{L}_2$ norm. The proposed approach computes a lower bound on the gain by restricting the parameter trajectory to be a periodic signal. This restriction enables the use of recent results for exact calculation of the $\mathcal{L}_2$ norm for a periodic linear time varying system. The proposed lower bound algorithm returns also a worst-case parameter trajectory for the LPV system that can be further analyzed to provide insight into the system performance.

Received . . .

KEY WORDS: Linear parameter varying systems, induced $\mathcal{L}_2$ norm, periodic linear time-varying systems

1. INTRODUCTION

The induced $\mathcal{L}_2$ norm of an LPV system is an important performance metric for control design. In general, this norm cannot be determined exactly. Most prior work focuses on computing an upper bound on the induced $\mathcal{L}_2$ norm. The method used to compute the induced gain upper bound depends primarily on the structure of the LPV system. For LFT-type LPV systems, where the system matrices are rational functions of the parameter, the upper bound can be computed using scaled small gain theorems with multipliers and the full block S-procedure [1, 2]. For LPV systems where the parameter dependence is arbitrary, the upper bound is computed using a dissipation inequality evaluated over a finite set of parameter grid points [3, 4, 5].

This paper addresses the complementary problem: calculation of a lower bound on the induced $\mathcal{L}_2$ norm. Frozen point analysis is one simple way to compute a lower bound. Specifically, a lower bound is computed as the maximum gain of LTI systems obtained by evaluating the LPV system on a grid of frozen parameter values. To our knowledge this is the only method currently available to compute a lower bound on the induced $\mathcal{L}_2$ norm of an LPV system. Unfortunately, this approach produces conservative results in many cases as it neglects the variation of the scheduling parameter.

*Correspondence to: Tamas Peni, Systems and Control Laboratory of Institute for Computer Science and Control, 1111 Budapest, Kende u. 13-17., Hungary, E-mail: pt@scl.sztaki.hu

A better estimate requires the $\mathcal{L}_2$ norm to be evaluated over time varying parameter trajectories. This introduces a complex optimization problem involving a maximization over the allowable parameter trajectories and the $\mathcal{L}_2$ inputs to the LPV system.

The proposed lower bound algorithm restricts the scheduling trajectories to periodic signals. This restriction is useful because the LPV system evaluated on a fixed periodic trajectory is simply a periodic linear time-varying (PLTV) system. Moreover, the induced $\mathcal{L}_2$ norm of a PLTV system can be exactly determined by using recently developed numerical methods, see e.g. [6]. The proposed algorithm entails maximizing a cost function related to the induced $\mathcal{L}_2$ norm (described in detail in Sec. 3) over a finite dimensional subspace of periodic scheduling trajectories. This produces a lower bound estimate and a worst-case parameter trajectory for the LPV system. In addition, we construct a worst-case input signal that approximately achieves the computed induced gain lower bound. The construction of the worst-case input is based on the PLTV results collected in [7] and [8]. In [7] the worst case input is derived by using a special, frequency domain representation for the PLTV system. In this paper the worst-case input construction and proofs are provided using time-domain operators only. This difference is analogous to the LTI case where the worst-case (steady-state) input is a sinusoid constructed based on frequency-domain considerations. In contrast, a time-domain argument addresses initial condition transients and yields a truncated sinusoid that approximately achieves the system gain. Similarly, the alternative time-domain approach for PLTV systems, detailed in section 2.3, yields signals (w^o, z^o) such that: (i) $w^o \in \mathcal{L}_2$, (ii) (w^o, z^o) is an input/output pair of the PLTV system G assuming zero initial conditions (including the transient response), and (iii) the gain of this input/output pair is within $\epsilon > 0$ of the induced $\mathcal{L}_2$ gain of G. These input/output signals (along with the parameter trajectory of the corresponding LPV system) can then be returned to user for further investigation, e.g. in a high fidelity simulation.

It is notable that our algorithm assumes no specific structure on the LPV system. Thus, it is developed for the systems with arbitrary parameter dependence. It trivially applies for "LFT" models as well, although the additional rational structure in LFT models may lead to faster lower bound algorithms than those developed here. This paper builds on initial work in [9]. This paper provides a full description for the lower bound algorithm including the worst-case input construction.

The notations used in the paper are fairly standard. $\mathbb{D}$ and $\partial\mathbb{D}$ are the unit disc and unit circle in the complex plane $\mathbb{C}$. If $\mathbf{T} : E \to F$ is a bounded, linear operator between Hilbert spaces E and F, then the adjoint of $\mathbf{T}$ is denoted by $\mathbf{T}^*$ and is defined as follows: $\langle \mathbf{T}u, y\rangle_F = \langle u, \mathbf{T}^* y\rangle_E$, $\forall u \in E$ and $\forall y \in F$. The space of square-integrable signals $f : [0, \infty) \to \mathbb{R}^n$ is denoted by $\mathcal{L}_2(\mathbb{R}^n)$. The inner product and norm in $\mathcal{L}_2(\mathbb{R}^n)$ are defined as $\langle f, g\rangle_{\mathcal{L}_2(\mathbb{R}^n)} = \int_0^\infty f(t)^T g(t)dt$ and $\|f\| = \sqrt{\langle f, f\rangle_{\mathcal{L}_2(\mathbb{R}^n)}}$, respectively. If $\mathbf{G}$ is a bounded linear operator, such that $\mathbf{G} : w \in \mathcal{L}_2(\mathbb{R}^p) \mapsto z \in \mathcal{L}_2(\mathbb{R}^q)$ then its induced $\mathcal{L}_2$ norm is defined as $\|\mathbf{G}\| := \sup_{0 \neq w \in \mathcal{L}_2(\mathbb{R}^p)} \frac{\|z\|}{\|w\|}$. $\mathcal{L}_{2,[0,h)}(\mathbb{R}^n)$ denotes the space of square-integrable functions on the interval $[0, h)$ with inner product $\langle f, g\rangle_{\mathcal{L}_{2,[0,h)}(\mathbb{R}^n)} = \int_0^h f(t)^T g(t)dt$. $\ell_2(E)$ denotes the square-summable sequences $w = \{w_k\}_{k=0}^\infty$ in the Hilbert space E with inner product $\langle w, v\rangle_{\ell_2(E)} := \sum_{k=0}^\infty \langle w_k, v_k\rangle_E$. If f is a signal $f : \mathbb{R} \to \mathbb{R}^n$, then $f(\cdot)$ refers to the entire signal while $f(t)$ denotes its value at t.

2. PERIODIC SYSTEMS

2.1. Background

This section reviews known results on PLTV systems. Most results can be found in [8]. In particular, we consider a linear time-varying system G of the form:

$$G : \quad \begin{array}{rcl} \dot{x}(t) & = & A(t)x(t) + B(t)w(t) \\ z(t) & = & C(t)x(t) + D(t)w(t) \end{array} \tag{1}$$

that has the following properties:

(i) the system matrices $A(t) : \mathbb{R} \to \mathbb{R}^{n\times n}$, $B(t) : \mathbb{R} \to \mathbb{R}^{n\times p}$, $C(t) : \mathbb{R} \to \mathbb{R}^{q\times n}$, $D(t) : \mathbb{R} \to \mathbb{R}^{q\times p}$ are bounded continuous functions of time,

DOI: 10.1002/rnc

(ii) are h-periodic, i.e. $A(t+h)=A(t), B(t+h)=B(t), C(t+h)=C(t), D(t+h)=D(t), \forall t$ and

(iii) the dynamics (1) are internally stable.

The state transition matrix $\Phi(t,\tau)$ associated with the autonomous dynamics $\dot{x}(t)=A(t)x(t)$ is defined for all (t,τ) as the linear mapping from $x(\tau)$ to $x(t)$, i.e. $x(t)=\Phi(t,\tau)x(\tau)$. It is easy to check that $\Phi(t,\tau)$ is periodic with h, i.e. $\Phi(t+h,\tau+h)=\Phi(t,\tau)$, and satisfies the matrix differential equation $\frac{d}{dt}\Phi(t,\tau)=A(t)\Phi(t,\tau)$, $\Phi(\tau,\tau)=I$. The state transition matrix over one period is called the monodromy matrix: $\Psi(t):=\Phi(t+h,t)$. Clearly, the monodromy matrix is periodic with h, i.e. $\Psi(t+h)=\Psi(t)$.

The system (1) is stable and hence it defines a bounded operator $\mathbf{G}:=w\in\mathcal{L}_2(\mathbb{R}^p)\mapsto z\in\mathcal{L}_2(\mathbb{R}^q)$, such that

$$z(t)=\int_0^t C(t)\Phi(t,\tau)B(\tau)w(\tau)\,d\tau+D(t)w(t) \tag{2}$$

where $z(t)$ is the response of (1) to the input $w(t)$ if $x(0)=0$. It is shown in [10] that $\|\mathbf{G}\|$ is equal to the norm of the "lifted" operator $\hat{\mathbf{G}}:\ell_2(\mathcal{L}_{2,[0,h)}(\mathbb{R}^p))\to\ell_2(\mathcal{L}_{2,[0,h)}(\mathbb{R}^q))$, which has a finite dimensional state-space realization as follows [11]:

$$\begin{aligned}\xi_{k+1}&=\hat{A}\xi_k+\hat{B}\hat{w}_k\\ \hat{z}_k&=\hat{C}\xi_k+\hat{D}\hat{w}_k\end{aligned} \tag{3}$$

where $\xi_k\in\mathbb{R}^n$ and $\hat{A}:\mathbb{R}^n\to\mathbb{R}^n$, $\hat{B}:\mathcal{L}_{2,[0,h)}(\mathbb{R}^p)\to\mathbb{R}^n$, $\hat{C}:\mathbb{R}^n\to\mathbb{R}^q$, $\hat{D}:\mathcal{L}_{2,[0,h)}(\mathbb{R}^p)\to\mathcal{L}_{2,[0,h)}(\mathbb{R}^q)$ are linear operators defined as follows:

$$\begin{aligned}\hat{A}\xi_k&:=\Psi(0)\xi_k, & \hat{B}\hat{w}_k&:=\int_0^h\Phi(h,\tau)B(\tau)\hat{w}_k(\tau)d\tau\\ \hat{C}\xi_k&:=C(t)\Phi(t,0)\xi_k, & \hat{D}\hat{w}_k&:=\int_0^t C(t)\Phi(t,\tau)\hat{w}_k(\tau)d\tau+D(t)\hat{w}_k(t).\end{aligned} \tag{4}$$

Although (3) is a finite dimensional system, it is still not suitable for numerical computations because its system matrices are operators. Therefore, based on Lemma 21.11 and Theorem 21.12 on pg. 539 of [12] the feedthrough term $\hat{D}$ is eliminated and a discrete-time, linear, time-invariant system $\underline{G}_\gamma$ is constructed from (3) ([13, 6]). The state-space matrices of $\underline{G}_\gamma$ are computed as follows:

$$\begin{aligned}\underline{A}_\gamma&:=\hat{A}+\hat{B}(\gamma^2I-\hat{D}^*\hat{D})^{-1}\hat{D}^*\hat{C}\\ \underline{B}_\gamma\underline{B}_\gamma^*&:=\gamma\hat{B}(\gamma^2I-\hat{D}^*\hat{D})^{-1}\hat{B}^*\\ \underline{C}_\gamma^*\underline{C}_\gamma&:=\gamma\hat{C}^*(\gamma^2I-\hat{D}\hat{D}^*)^{-1}\hat{C}.\end{aligned} \tag{5}$$

More specifically, the matrices $\underline{B}_\gamma$ and $\underline{C}_\gamma$ are defined to be full rank matrices that satisfy the equalities that appear in (5). Note that $\underline{A}_\gamma,\underline{B}_\gamma,\underline{C}_\gamma$ are now real matrices: $\underline{A}_\gamma\in\mathbb{R}^{n\times n},\underline{B}_\gamma\in\mathbb{R}^{n\times p},\underline{C}_\gamma\in\mathbb{R}^{q\times n}$. The following theorem, taken from [6], proves that there is a strong relation between the induced ℓ_2-norm of the LTI system $\underline{G}_\gamma$ and the norm of $\hat{\mathbf{G}}$.

Theorem 1
The following statements are equivalent:

a) $\mathrm{eig}(\hat{A})\in\mathbb{D}\backslash\partial\mathbb{D}$ and $\|\hat{\mathbf{G}}\|<\gamma$

b) $\mathrm{eig}(\underline{A}_\gamma)\in\mathbb{D}\backslash\partial\mathbb{D}$ and $\|\underline{G}_\gamma\|_\infty<1$

where $\|\underline{G}_\gamma\|_\infty$ is the standard $\mathcal{H}_\infty$ norm of $\underline{G}_\gamma$.

DOI: 10.1002/rnc

2.2. *Induced norm computation*

Theorem 1 gives the base of the bisection algorithm proposed in [6] to compute the $\mathcal{L}_2$-norm of the periodic system (1). This requires a numerically reliable method to determine the system matrices $\underline{A}_\gamma, \underline{B}_\gamma, \underline{C}_\gamma$. For this, consider the following Hamiltonian system associated with (1):

$$\dot{e}(t) = H(t)e(t) \tag{6}$$

where H has 2×2 blocks defined as (suppressing the notation of time dependence)

$$\begin{aligned} H_{11} &:= -A^T - C^T D(\gamma^2 I - D^T D)^{-1} B^T \\ H_{12} &:= -\gamma C^T (\gamma^2 I - DD^T)^{-1} C \\ H_{21} &:= \gamma B(\gamma^2 I - D^T D)^{-1} B^T \\ H_{22} &:= A + B(\gamma^2 I - D^T D)^{-1} D^T C. \end{aligned} \tag{7}$$

Denote the monodromy matrix of (6) by $\Psi_H(t)$ and let $Q = \Psi_H(0)$. Partitioning $Q = \left[\begin{smallmatrix} Q_{11} & Q_{12} \\ Q_{21} & Q_{22} \end{smallmatrix}\right]$ yields [6]

$$\begin{aligned} \underline{B}_\gamma \underline{B}_\gamma^T &= Q_{21} Q_{11}^{-1} \\ \underline{C}_\gamma^T \underline{C}_\gamma &= -Q_{11}^{-1} Q_{12} \\ \underline{A}_\gamma &= Q_{22} - Q_{21} Q_{11}^{-1} Q_{12}. \end{aligned} \tag{8}$$

Q is symplectic [14], i.e. $Q^T J Q = J$, and thus Q is uniquely determined by (8) in the following form:

$$Q = \begin{bmatrix} \underline{A}_\gamma^{-T} & -\underline{A}_\gamma^{-T} \underline{C}_\gamma^T \underline{C}_\gamma \\ \underline{B}_\gamma \underline{B}_\gamma^T \underline{A}_\gamma^{-T} & \underline{A}_\gamma - \underline{B}_\gamma \underline{B}_\gamma^T \underline{A}_\gamma^{-T} \underline{C}_\gamma^T \underline{C}_\gamma \end{bmatrix}. \tag{9}$$

A possible method to compute $\underline{A}_\gamma, \underline{B}_\gamma, \underline{C}_\gamma$ can be given as follows. First integrate the Hamiltonian system (6) on $[0, h)$ from the matrix initial condition $e(0) = I$. Then $Q = e(h)$. Determine the system matrices from Q using (8). Since $H(t)$ is unstable this approach is numerically unreliable. An alternative method proposed in [6] is based on the following relations:

$$\underline{A}_\gamma = X(h), \quad \underline{C}_\gamma^T \underline{C}_\gamma = Z(0), \quad \underline{B}_\gamma \underline{B}_\gamma^T = Y(h) \tag{10}$$

where $X(h)$, $Z(0)$, and $Y(h)$ are point solutions of the differential Riccati equations

$$\dot{Z} = -H_{22}^T Z - Z H_{22} - \gamma Z B(\gamma^2 I - D^T D)^{-1} B^T Z + \gamma C^T (\gamma^2 I - DD^T)^{-1} C \tag{11}$$

$$\dot{X} = (H_{22} + \gamma B(\gamma^2 I - D^T D)^{-1} B^T Z) X \tag{12}$$

$$\dot{Y} = H_{22} Y + Y H_{22}^T + \gamma Y C^T (\gamma^2 I - DD^T)^{-1} C Y + \gamma B(\gamma^2 I - D^T D)^{-1} B^T \tag{13}$$

with boundary conditions $Z(h) = 0, X(0) = I$ and $Y(0) = 0$. Integrating these Riccati equations is a numerically better conditioned problem than the direct integration of (6) [6]. The bisection algorithm proposed in [6] is based on iteratively solving (11)-(13) and computing $\|\underline{G}_\gamma\|_\infty$ at different γ values that are tuned in a bisection loop. The output is a lower- and upper bound pair $(\underline{\gamma}, \overline{\gamma})$ satisfying $\underline{\gamma} \le \|\mathbf{G}\| \le \overline{\gamma}$ such that $\overline{\gamma} - \underline{\gamma} \le \varepsilon$, where ε is a given tolerance.

Remark 1
If we introduce $T = \left[\begin{smallmatrix} 0 & I \\ \gamma I & 0 \end{smallmatrix}\right]$ and apply the state transformation $\tilde{e}(t) = T^{-1} e(t)$ in (6), we get the following transformed Hamiltonian system:

$$\dot{\tilde{e}}(t) = \tilde{H}\tilde{e}(t), \quad \text{with} \quad \tilde{H}(t) = T^{-1} H(t) T. \tag{14}$$

This system is the same as that used in [7]. Denote $\Psi_{\tilde{H}}(t)$ as the monodromy matrix associated with (14) and let $\tilde{Q} := \Psi_{\tilde{H}}(0)$. Then, it can be shown that $\tilde{Q} = T^{-1} Q T$. We use (14) instead of (6) in the next section, because (14) is more convenient for the forthcoming derivations.

DOI: 10.1002/rnc

2.3. *Construction of the worst-case input*

We are also interested in constructing the worst-case input $w^\circ \in \mathcal{L}_2$ that achieves the induced norm $\|\mathbf{G}\|$. It is shown that the input signal producing the induced norm is periodic, thus it is not in $\mathcal{L}_2$. Hence, the method we provide can only approximately achieve this gain. Specifically, for any $\epsilon > 0$ we construct an input $w^\circ \in \mathcal{L}_2$ such that $z^\circ := \mathbf{G}w^\circ$ satisfies $\|z^\circ\| \geq \|\mathbf{G}\|\|w^\circ\| - \epsilon$. This is similar to the LTI case where the worst-case input is a sinusoid and a truncated sinusoid approximately achieves the system gain. The method used to construct the worst-case input for the PLTV system is based on the proof of Lemma 2.6 in [7]. In [7] the worst-case input is constructed using a special frequency-domain representation of $\mathbf{G}$ defined over exponentially periodic signals. In this section, an alternative construction and proof is provided using only time-domain formulations. This alternative proof streamlines the numerical construction of the worst-case input. To this end, let the linear operator $\mathbf{T}_G : \mathbb{R}^n \times \mathcal{L}_{2,[0,h)}(\mathbb{R}^p) \to \mathbb{R}^n \times \mathcal{L}_{2,[0,h)}(\mathbb{R}^q)$ be defined as follows:

$$\mathbf{T}_G(x_0, w) \to (x_h, z) := (\hat{A}x_0 + \hat{B}w,\ \hat{C}x_0 + \hat{D}w).$$

$\mathbf{T}_G$ is equivalent to the (state-input) $\to$ (state-output) map realized by (1) over the period $[0, h)$ with $x(0) = x_0$, $x_h = x(h)$. Introduce an inner product on $\mathbb{R}^n \times \mathcal{L}_{2,[0,h)}(\mathbb{R}^\cdot)$ as

$$\langle (x, w), (y, v) \rangle = x^* y + \int_0^h w^*(t)v(t)dt.$$

Then the adjoint operator $\mathbf{T}_G^*$ is defined to satisfy the equation

$$\langle (\hat{x}_h, \hat{z}), \mathbf{T}_G(x_0, w) \rangle = \langle \mathbf{T}_G^*(\hat{x}_h, \hat{z}), (x_0, w) \rangle.$$

The next lemma provides a state-space realization for the adjoint operator.

Lemma 1
If $(\hat{x}_0, \hat{w}) = \mathbf{T}_G^*(\hat{x}_h, \hat{z})$ then

$$\begin{aligned} \dot{\hat{x}}(t) &= -A^*(t)\hat{x}(t) - C^*(t)\hat{z}(t), \quad \hat{x}(h) = \hat{x}_h \\ \hat{w}(t) &= B^*(t)\hat{x}(t) + D^*(t)\hat{z}(t), \quad \hat{x}_0 = \hat{x}(0). \end{aligned} \tag{15}$$

Proof
The proof is provided in the Appendix. □

The following lemma provides a useful interpretation for the Hamiltonian dynamics (14) in terms of the operator $\mathbf{T}_G$ and its adjoint.

Lemma 2
Interconnect the dynamics of (1) and (15) with $\hat{z}(t) := z(t)$ and $w(t) := \gamma^{-2}\hat{w}(t)$. The resulting autonomous dynamics has state $\tilde{e}^T := [x^T\ \hat{x}^T]$ with dynamics given by (suppressing dependence on t):

$$\dot{\tilde{e}} = \tilde{H}\tilde{e} \tag{16}$$

$$w = (\gamma^2 I - D^*D)^{-1} \begin{bmatrix} D^*C & B^* \end{bmatrix} \tilde{e} \tag{17}$$

$$z = (\gamma^2 I - DD^*)^{-1} \begin{bmatrix} \gamma^2 C & DB^* \end{bmatrix} \tilde{e}. \tag{18}$$

Moreover let (λ, v) denote an eigenvalue/eigenvector of the monodromy matrix $\tilde{Q}$ for (16). Partition $v^* := [v_1^*\ v_2^*]$ conformably with the state $\tilde{e}^T := [x^T\ \hat{x}^T]$. Then $\mathbf{T}_G(v_1, w) = (\lambda v_1, z)$ and $\mathbf{T}_G^*(\lambda v_2, z) = (v_2, \gamma^2 w)$.

Proof
The expression for the Hamiltonian dynamics as the feedback connection of (1) and (15) is from [7]. The remaining relations follow from the definitions of $\mathbf{T}_G$ and $\mathbf{T}_G^*$. □

DOI: 10.1002/rnc

Next, we show that the worst-case input can be constructed from (17) if the Hamiltonian system (16) is initialized as $\tilde{e}(0) = v$. This requires the following result which is a direct consequence of Lemma 21.10 in [12]:

Theorem 2
The following statements are equivalent:

(a) $\|\underline{G}_\gamma\|_\infty < 1$.

(b) $\tilde{Q}$ has no eigenvalues on $\partial\mathbb{D}$ and there exists $\theta \in [0, \pi]$ such that $\sigma_{\max}(\underline{G}_\gamma(e^{j\theta})) < 1$.

Theorems 1 and 2 imply that if $\gamma < \|\mathbf{G}\|$, i.e. $\|\underline{G}_\gamma\|_\infty \geq 1$ then $\tilde{Q}$ has a unit modulus eigenvalue or $\sigma_{\max}(\underline{G}_\gamma(e^{j\theta})) \geq 1$ for all $\theta \in [0, \pi]$. If the latter occurs with strict inequality then $\tilde{Q}$ does not have an eigenvalue on $\partial\mathbb{D}$. If this is the case, γ can be slightly increased to find $\gamma_1 > \gamma$ such that $\gamma_1 \leq \|\mathbf{G}\|$ and $\sigma_{\max}(\underline{G}_{\gamma_1}(e^{j\theta_1})) \leq 1$ for some $\theta_1 \in [0, \pi]$. The existence of such a γ_1 follows from the fact that $\sigma_{\max}(\underline{G}_\gamma(e^{j\theta}))$ is continuous in γ and from Theorem 2 saying that if γ is increased until it exceeds the norm of $\mathbf{G}$ then there is a frequency, where the maximal singular value is smaller than 1. By using the argument in the proof of Lemma 21.10 in [12], $\|\underline{G}_{\gamma_1}\|_\infty \geq 1$ together with $\sigma_{\max}(\underline{G}_{\gamma_1}(e^{j\theta_1})) \leq 1$ implies that $\tilde{Q}$ has a unit modulus eigenvalue. Note that, if the reasoning above is applied with the norm bound γ computed by the bisection algorithm introduced in the previous subsection then it is easy to see that $\gamma_1 \in [\underline{\gamma}, \|\mathbf{G}\|]$, i.e. the increment $\gamma_1 - \underline{\gamma}$ is indeed small, less than the tolerance ε. It is also important to note that the case of $\tilde{Q}$ having no unit modulus eigenvalue is unlikely to be encountered in practice, since the stopping tolerance is always reasonably tight. (We tested the bisection algorithm on many examples, and we did not face this problem so far.)

Let γ be such that $\gamma < \|\mathbf{G}\|$ and $\tilde{Q}$ has a unit modulus eigenvalue. Let v denote the corresponding eigenvector. Let $\tilde{e}$ denote the solution of the Hamiltonian dynamics (16) and (w, z) the corresponding outputs with initial condition $\tilde{e}(0) = v$. Then Lemma 2 implies that $\mathbf{T}_G$ maps the input w and initial state v_1 to the output z and final state $e^{j\omega h}v_1$. It also follows from Lemma 2 that:

$$\begin{aligned} v_2^* v_1 + \int_0^h z^*(t)z(t) &= \langle (e^{j\omega h}v_2, z), \mathbf{T}_G(v_1, w)\rangle \\ &= \langle \mathbf{T}_G^*(e^{j\omega h}v_2, z), (v_1, w)\rangle \\ &= v_2^* v_1 + \gamma^2 \int_0^h w^*(t)w(t) \end{aligned} \tag{19}$$

Thus $||z||_{[0,h)} = \gamma||w||_{[0,h)}$, i.e. the $\mathcal{L}_2$ gain of $\mathbf{G}$ is equal to γ on the interval $[0, h)$ provided the initial condition of the system $\mathbf{G}$ is given by $x(0) = v_1$.

Note that the input/output pair (w, z) for $t \in [0, h)$ is obtained by integrating the Hamiltonian dynamics (16) starting from $\tilde{e}(0) = v$. The state after one period is given by $\tilde{e}(h) = \tilde{Q}\tilde{e}(0) = e^{j\omega h}v$. Thus integrating the periodic Hamiltonian dynamics forward over the next interval yields $w(t) = e^{j\omega h}w(t-h)$ and $z(t) = e^{j\omega h}z(t-h)$ for $t \in [h, 2h)$. Continuing to evolve the Hamiltonian dynamics forward in time over subsequent periodic intervals yields an input/output pair of $\mathbf{G}$ such that for any interval $k \in \{0, 1, 2, \ldots\}$:

$$w(t) = e^{j\omega kh}w(t - kh), \quad t \in [kh, (k+1)h) \tag{20}$$

$$z(t) = e^{j\omega kh}z(t - kh). \tag{21}$$

This input/output pair satisfies $\|z\|_{[kh,(k+1)h)} = \gamma\|w\|_{[kh,(k+1)h)}$ over each interval $[kh, (k+1)h)$. Thus w is, loosely speaking, an input that achieves the gain γ. There are three issues to be resolved to make this more precise. First, the input (20) is persistent and hence is not in $\mathcal{L}_{2,[0,\infty)}$. Second, the signals (w, z) in (20-21) are an input/output pair of $\mathbf{G}$ only if the periodic system starts with the initial condition $x(0) = v_1$. However, the induced gain is defined assuming $x(0) = 0$. Third, the input can be complex if the eigenvector v is complex.

DOI: 10.1002/rnc

The first two issues are resolved by noting that (w, z) defined by (20-21) can be expressed using the state transition matrix as:

$$z(t) = C(t)\Phi(t,0)v_1 + \int_0^t C(t)\Phi(t,\tau)B(\tau)w(\tau)\,d\tau + D(t)w(t). \tag{22}$$

Define $w^\bullet$ as the truncation of w after K periodic intervals, i.e. $w^\bullet(t) := w(t)$ for $t \in [0, Kh)$ and $w^\bullet(t) := 0$ otherwise. Define $z^\bullet$ as the output of $\mathbf{G}$ driven by input $w^\bullet$ but with initial condition $x(0) = 0$. Then $z^\bullet(t) = z(t) - s(t)$ for $t < Kh$ where $s(t) := C(t)\Phi(t,0)v_1$ is the initial condition response. The norm of $z^\bullet$ can be bounded as:

$$\|z^\bullet\| \geq \|z\|_{[0,Kh)} - \|s\|_{[0,Kh)} = \gamma\|w^\bullet\|_{[0,Kh)} - \|s\|_{[0,Kh)}. \tag{23}$$

The first inequality follows from the triangle inequality. The second equality follows from two facts. First, $\|z\|_{[kh,(k+1)h)} = \gamma\|w\|_{[kh,(k+1)h)}$ over each interval as noted above. Second, $w^\bullet = w$ by construction for $t \in [0, Kh)$. Next note that $\|s\|_{[0,Kh)} \leq \|s\| < \infty$ due to the stability of $\mathbf{G}$. In addition, $\|w^\bullet\|_{[0,Kh)} = K\|w^\bullet\|_{[0,h)}$ and hence $\|w^\bullet\|_{[0,Kh)} \to \infty$ as $K \to \infty$. Thus it is clear that $\forall \epsilon > 0$ there exists an integer K such that the input-output pair $(w^\bullet, z^\bullet)$ of $\mathbf{G}$ satisfies $\frac{\|z^\bullet\|}{\|w^\bullet\|} \geq \gamma - \epsilon$. The input $w^\bullet$ is a valid "worst-case" signal because it is in $\mathcal{L}_2$ and the output has been generated with zero initial conditions.

The remaining issue is the fact that $(w^\bullet, z^\bullet)$ may be complex. The periodic system $\mathbf{G}$ is linear and the system matrices are real. Thus neglecting the imaginary part of the complex valued input does not change the gain. Therefore the real valued worst-case input can be obtained by $w^\circ = Re(w^\bullet)$. Now we can summarize the complete algorithm.

Algorithm 1 (Worst-case input)

1: Let $\underline{\gamma}$ be given such that $\underline{\gamma} \leq \|\mathbf{G}\|$. Set $\gamma := \underline{\gamma}$.
2: Compute Q from $\underline{A}_\gamma, \underline{B}_\gamma, \underline{C}_\gamma$ using the equation (9). Determine $\tilde{Q}$ by applying the similarity transformation T.
3: Compute the unit modulus eigenvalue $e^{j\omega h}$ of $\tilde{Q}$ and the corresponding eigenvector v. (If $\tilde{Q}$ does not have a unit modulus eigenvalue, then increase γ according to the discussion after Theorem 2 and restart the algorithm with the new value obtained.)
4: Integrate the Hamiltonian dynamics (14) from $t = 0$ to $t = h$ starting from the initial condition $\tilde{e}(0) = v$.
5: Use (17) to compute $w(t)$ on $[0, h)$ from $\tilde{e}(t)$.
6: Choose an integer $K \gg 1$ and define the (possibly complex valued) signal $w^\bullet(t)$ by: $w^\bullet(t) = e^{j\omega kh}w(t - kh)$ if $t \in [kh, (k+1)h)$, $k = 0, 1, \ldots, K-1$ and $w^\bullet(t) = 0$ if $t \geq Kh$.
7: Let $w^\circ := \mathrm{Re}(w^\bullet)$ and $z^\circ := \mathbf{G}w^\circ$.

Remark 2
If h is "too large", the integration of the Hamiltonian system in step 4 of Algorithm 1 may cause numerical problems, because the Hamiltonian system is unstable. If this is the case, then aligned with the ideas in [6], an alternative, numerically more reliable method can be applied to determine the $\tilde{e}(t)$ trajectory for all $t \in [0, h)$. This method is based on constructing the state transition matrix $\tilde{\Phi}(\tau, 0)$ of (14) for all $\tau \in [0, h)$ by using the Riccati equations (11)-(13). For this, let $\tau \in [0, h)$ and denote $X(\tau), Z(0)$ and $Y(\tau)$ the point solutions obtained by solving equations (11)-(13) with boundary conditions $Z(\tau) = 0, X(0) = I$ and $Y(0) = 0$. Then, analogously to equations (10), we can define $A_{\gamma,\tau}, B_{\gamma,\tau}, C_{\gamma,\tau}$ to satisfy $\underline{A}_{\gamma,\tau} = X(\tau)$, $\underline{C}^T_{\gamma,\tau}\underline{C}_{\gamma,\tau} = Z(0)$, $\underline{B}_{\gamma,\tau}\underline{B}^T_{\gamma,\tau} = Y(\tau)$. By substituting these matrices into equation (9) the state transition matrix $\Phi(\tau, 0)$ can be obtained. Finally, let $\tilde{\Phi}(\tau, 0) = T^{-1}\Phi(\tau, 0)T$ and $\tilde{e}(\tau) = \tilde{\Phi}(\tau, 0)\tilde{e}(0) = \tilde{\Phi}(\tau, 0)\tilde{v}$ for all $\tau \in [0, h)$.

DOI: 10.1002/rnc

3. COMPUTATION OF LOWER BOUNDS FOR THE INDUCED $\mathcal{L}_2$ NORM OF LPV SYSTEMS

3.1. Problem formulation

The linear parameter-varying system is assumed to be given in state-space form as follows:

$$G: \quad \begin{array}{rcl} \dot{x}(t) & = & A(\rho(t))x(t) + B(\rho(t))w(t) \\ z(t) & = & C(\rho(t))x(t) + D(\rho(t))w(t) \end{array} \tag{24}$$

where the system matrices are continuous functions of the parameter ρ. In addition, $\rho(\cdot)$ is a piecewise continuously differentiable function of time, $\rho : \mathbb{R}^+ \to \mathbb{R}^m$, that is assumed to satisfy the known bounds

$$\underline{\rho_i} \leq \rho_i(t) \leq \overline{\rho}_i, \;\; \underline{\mu_i} \leq \dot{\rho}_i(t) \leq \overline{\mu}_i, \; \forall t, \; 1 \leq i \leq m \tag{25}$$

The set of admissible trajectories containing all piecewise continuously differentiable trajectories that satisfy (25) is denoted by $\mathcal{A}$. The performance of an LPV system G can be specified in terms of its induced $\mathcal{L}_2$ gain from input w to output z assuming $x(0) = 0$: $\|G\| = \sup_{0 \neq w \in \mathcal{L}_2(\mathbb{R}^p), \rho(\cdot) \in \mathcal{A}} \frac{\|z\|}{\|w\|}$.

3.2. Lower bound for the induced $\mathcal{L}_2$ norm

The computation of the lower bound is based on restricting the scheduling parameter trajectories to a finite-dimensional set of periodic signals. Let $\rho : \mathbb{R}^+ \times \mathbb{R}^N \to \mathbb{R}^m$ denote a function that specifies a periodic scheduling trajectory for each value of $c \in \mathbb{R}^N$. $\rho(\cdot, c)$ denotes the entire trajectory (as a function of time) at the particular value c and $\rho(t, c)$ denotes the m-dimensional scheduling vector obtained by evaluating $\rho(\cdot, c)$ at time instant t. The trajectory is assumed to be periodic, i.e. for each c there is a period $h(c)$ such that $\rho(t + h(c), c) = \rho(t, c)$ $\forall t$. In addition, we must ensure the trajectory is admissible in the sense that it satisfies the range and rate bounds in (25). Let $\mathcal{C}_p \subseteq \mathbb{R}^N$ denote the set of values that lead to such admissible trajectories, i.e. $\rho(\cdot, c) \in \mathcal{A}$ for all $c \in \mathcal{C}_p$. The corresponding set of periodic trajectories is defined as $\mathcal{A}_p := \{\rho(\cdot, c) \,|\, c \in \mathcal{C}_p\}$.

Define the lower bound γ_{lb} on the induced $\mathcal{L}_2$ gain as

$$\gamma_{lb} := \sup_{\rho(\cdot,c) \in \mathcal{A}_p} \|\mathbf{G}_{\rho(\cdot,c)}\| = \sup_{c \in \mathcal{C}_p} \|\mathbf{G}_{\rho(\cdot,c)}\| \tag{26}$$

where $\mathbf{G}_{\rho(\cdot,c)}$ denotes the periodic system (operator) obtained by evaluating the LPV system G along the periodic trajectory $\rho(\cdot, c)$. The algorithm described in [6] can be used to evaluate the gain $\|\mathbf{G}_{\rho(\cdot,c)}\|$. It follows immediately from $\mathcal{A}_p \subset \mathcal{A}$ that $\gamma_{lb} \leq \|G\|$. Equation (26) defines a finite dimensional optimization problem which is non-convex in general. One further issue is that a single, accurate evaluation of $\|\mathbf{G}_{\rho(\cdot,c)}\|$ requires many bisection steps and, as a consequence, the matrix differential equations (Equations (12), (13) and (11)) must be integrated many times for a single evaluation of the objective function. Thus the evaluation of $\|\mathbf{G}_{\rho(\cdot,c)}\|$ is costly and a significant reduction in computation can be achieved by using Algorithm 2 described below. In this algorithm, $\underline{G}_{\gamma,\rho(\cdot,c)}$ denotes the discrete-time system (5) corresponding to the PLTV operator $\mathbf{G}_{\rho(\cdot,c)}$. Moreover, define $\nu(c, \gamma) := \|\underline{G}_{\gamma,\rho(\cdot,c)}\|$. With this notation, $\|\mathbf{G}_{\rho(\cdot,c)}\| < \gamma$ if and only if $\nu(c, \gamma) < 1$. The lower bound algorithm can now be stated.

Algorithm 2 (Lower bound on $\mathcal{L}_2$ norm)

1: Compute an upper bound γ_{ub} on the gain of the LPV system, i.e. $\gamma_{ub} \geq \|G\|$. Such an upper bound can be determined using standard methods based on dissipation inequalities (e.g. Bounded Real type LMI conditions) [15], [4]. Pick an initial vector c_0.
2: Solve the optimization problem $c^* = arg\max_{c \in \mathcal{C}_p} \nu(c, \gamma_{ub})$. This is a nonlinear optimization problem, where the evaluation of the cost function requires the integration of the Riccati differential equations (11)-(13). Therefore to obtain c^*, a nonlinear optimization method (e.g. *pattern search* [16]) has to be applied. (It is important to note we cannot prove in general

DOI: 10.1002/rnc

that maximizing $\nu(c, \gamma_{ub})$ gives the same result as directly maximizing the norm of the periodic operator $\mathbf{G}_{\rho(\cdot,c)}$. In numerical examples we always found that the relation between the two quantities is monotonic, i.e. the larger the $\nu(c, \gamma_{ub})$, the larger the $\|\mathbf{G}_{\rho(\cdot,c)}\|$ is. The maximization of $\nu(c, \gamma_{ub})$ is thus a reasonable heuristics that works well in practice.)

3: Compute the norm of $\mathbf{G}_{\rho(\cdot,c^*)}$ and take $\underline{\gamma}$ from the outputs of the bisection. Let $\gamma_{lb} := \underline{\gamma}$ and stop.

This algorithm only requires the $\mathcal{L}_2$ norm of the periodic system to be evaluated at the last step. This significantly reduces the number of integrations for the matrix differential equations associated with X, Y, and Z. The output of the algorithm above is an induced gain lower bound γ_{lb} and a worst-case scheduling trajectory $\rho(\cdot, c^*)$ where the associated PLTV system takes this norm. By using Algorithm 1 we can also construct a worst-case input signal w^o for $\mathbf{G}_{\rho(\cdot,c^*)}$. This, together with $\rho(\cdot, c^*)$ gives a worst-case (input, scheduling trajectory) pair achieving an induced gain of γ_{lb}.

3.3. *Scheduling trajectories*

Algorithm 2 optimizes the $\mathcal{L}_2$ bound over the elements of $\mathcal{A}_p$. The structure of $\rho(\cdot, c)$ must be carefully chosen as it influences the convergence properties of the lower bound algorithm. There are many ways to construct periodic signals and this section focuses on piecewise linear scheduling trajectories. An alternative construction based on sinusoidal basis functions is described in the initial work [9].

Focusing on the one dimensional case ($n_\rho = 1$), the simplest way to define a periodic piecewise linear trajectory is dividing the period $[0, h)$ into N intervals of lengths $\Delta_1, \Delta_2, \ldots \Delta_N$ and then defining the N scheduling parameter values $\rho_i = \rho(t_i)$ $i = 1 \ldots N$ over the break points $t_1 = 0$, $t_2 = \Delta_1, \ldots t_i = \sum_{j=1}^{i-1} \Delta_j$, $i = 1 \ldots N$. By definition, $\sum_{j=1}^{N} \Delta_j = h$. If c is chosen to be

$$c = [\Delta_1, \Delta_2, \ldots, \Delta_N,\ \rho_1, \rho_2, \ldots, \rho_N]^T$$

then the magnitude and rate limits (25) can be transformed into linear constraints:

$$\begin{aligned} \underline{\rho} \le \rho_i \le \overline{\rho} & \\ \Delta_i \underline{\mu} \le \rho_{i+1} - \rho_i \le \Delta_i \overline{\mu}, & \quad \forall i < N \\ \Delta_N \underline{\mu} \le \rho_0 - \rho_N \le \Delta_N \overline{\mu} & \end{aligned}$$

Thus $\mathcal{C}_p$ is a polytope. Since h is a sum of the Δ_i interval-lengths, thus it is a free parameter, that can be tuned by the optimization algorithm. Note that by increasing N any piecewise continuously differentiable trajectory can be approximated up to any tolerance. In this sense, the parameterization is complete.

Remark 3
For numerical reasons, it makes sense to introduce an inequality constraint of the form $h \le \bar{h}$ to bound the period length when performing the optimization in the second step of Algorithm 2. This is simply another linear constraint on the vector c.

3.4. *Computational issues*

The computational complexity of Algorithm 2 is determined by two main factors. First, the cost function $\nu(c, \gamma_{ub})$ is nonlinear, so a nonlinear optimization method is needed, the convergence rate and computation demand of which is hard to predict; second, the evaluation of $\nu(c, \gamma_{ub})$ is computationally demanding as it requires the integration of the three Riccati equations (11)-(13). If T_r denotes the integration time and N_e is the number of times that the cost function is evaluated by the nonlinear optimization solver, the total computation time is roughly given by $N_e \cdot T_r$.

Assuming that an adaptive Runge-Kutta algorithm (e.g. *ode45* in MATLAB) is used for numerical integration, T_r is determined by three factors: (i) the number of states (n) determining the number of differential equations in (11)-(13), (ii) the actual trajectory $\rho(\cdot, c)$, which, if varies rapidly, requires a

DOI: 10.1002/rnc

small integration step size, and thus slows down the computation, (iii) the horizon h, which defines the time interval of integration.

The number of cost function evaluations (N_e) depends on the nonlinear optimization algorithm applied. By trying some gradient-based algorithms we found that they are very sensitive to the initial value of the decision variables and the gradient of the cost function is difficult to calculate. These algorithms easily run into a local minimum. Therefore, we have chosen the gradient-free, pattern search optimization method. This iterative algorithm is based on constructing M points (the mesh) around the actual parameter vector and finding (polling) one point, where the cost function is higher than the actual cost. The iteration is then repeated starting from this new point. If the selection fails, because there is no point in the mesh that improves the actual cost, then a new mesh is generated and the procedure repeats. If the algorithm is configured to run with maximal basis i.e. $M = 2N_c$ where N_c is the number of decision variables, and complete poll is applied (i.e. the cost function is always evaluated at all of the $2N_c$ points of the mesh, so the evaluation does not stop at the first good point) then $N_e = N_s \cdot 2N_c$, where N_s is the number of optimization steps. With minimal basis ($M = N_c + 1$) and non-complete poll, the total number of evaluations satisfies $N_e < N_s \cdot (N_c + 1)$. It can be seen that pattern search requires less evaluations at each step than the gradient-based algorithms, but it is also important to note that these methods need more optimization steps, i.e. N_s is higher, in general.

In the numerical simulations we applied the pattern search tools of MATLAB [16]. We found that these algorithms are less sensitive to the initial value and provide reliable solution to the optimization problem in Algorithm 2.

4. NUMERICAL EXAMPLES

In this section three numerical examples are presented to demonstrate the applicability of the proposed method. To initialize our algorithms we need to determine an upper bound γ_{ub} for the induced $\mathcal{L}_2$ gain. In all examples γ_{ub} is computed by solving the following optimization problem:

$$\begin{aligned} &\min_{V(x,\rho)} \gamma \\ &V(x,\rho) > 0, \dot{V}(x,\rho,\dot{\rho}) \leq \gamma^2 w^T w - z^T z \end{aligned} \tag{27}$$

where the Lyapunov (storage) function $V(x,\rho)$ was chosen to be quadratic: $V(x,\rho) = x^T P(\rho) x$, $P(\rho) = P(\rho, P_0, P_1, \ldots, P_M)$ and P_i-s denote the free (matrix) variables to be found. The infinite LMI constraints obtained were transformed to a finite set by choosing a suitable dense grid Γ over the parameter domain $\mathcal{P}$ and only the inequalities evaluated at the grid points are considered [3].

4.1. LPV system with gain-scheduled PI controller

The first example, taken from [17] is a feedback interconnection of a first-order LPV system with a gain-scheduled proportional-integral controller (see Fig. 1). The dynamics of the closed-loop system can be written as follows

$$\begin{aligned} \begin{bmatrix} \dot{x} \\ \dot{x}_c \end{bmatrix} &= \begin{bmatrix} -\frac{1}{\tau(\rho)}(1 + K_p(\rho)K(\rho)) & \frac{1}{\tau(\rho)} \\ -K_i(\rho)K(\rho) & 0 \end{bmatrix} \begin{bmatrix} x \\ x_c \end{bmatrix} + \begin{bmatrix} \frac{1}{\tau(\rho)}K_p(\rho) \\ K_i(\rho) \end{bmatrix} r \\ e &= [-K(\rho)\ 0] \begin{bmatrix} x \\ x_c \end{bmatrix} + r \end{aligned} \tag{28}$$

where $\tau(\rho) := \sqrt{13.6 - 16.8\rho}$, $K(\rho) := \sqrt{4.8\rho - 8.6}$ and

$$K_p(\rho) = \frac{2\xi_{cl}\omega_{cl}\tau(\rho) - 1}{K(\rho)}, \quad K_i(\rho) = \frac{\omega_{cl}^2 \tau(\rho)}{K(\rho)}.$$

The PI gains K_p and K_i are chosen to provide closed-loop damping $\xi_{cl} = 0.7$ and natural frequency $\omega_{cl} = 0.25$ at each frozen value of ρ. The scheduling parameter is assumed to vary in the interval

DOI: 10.1002/rnc

$[2, 7]$ and $\dot{\rho} \in [-1,\ 1]$. We are interested in the induced $\mathcal{L}_2$ norm between $r(t)$ and $e(t)$. By performing the optimization (27) with

$$V(x,\rho) = x^T \left(P_0 + \sum_{k=1}^{6} \rho^k P_k + \frac{1}{\rho} P_7 + \frac{1}{\rho^2} P_8 + \frac{1}{\rho^3} P_9 \right) x$$
$$\Gamma = \{\rho_1 = 2, \ldots, \rho_{100} = 7\},\ \ \rho_{k+1} - \rho_k = 5/99 \tag{29}$$

we got $\gamma_{ub} = 2.964$ for the upper bound. Using the parameter values in Γ the frozen lower bound was also computed as $\gamma_{lb,fr} = \max_k \|G_{\rho_k}\|$, $\rho_k \in \Gamma$, where G_{ρ_k} denotes the LTI system obtained by substituting $\rho(t) = \rho_k$ for all t. The lower bound we obtained is $\gamma_{lb,fr} = 1.1066$.

To compute the lower bound by Algorithm 2, we tuned $N = 4$ points of the piecewise linear scheduling trajectory. The algorithm was run with the additional constraint $h \in [h_{min}\ h_{max}] = [12\ 20]$. The nonlinear optimization was performed under MATLAB, by using the pattern search algorithm implemented in the Global Optimization Toolbox [16]. The computation time was approx. $310s$. The algorithm terminated with $\gamma_{lb} = 2.8362$ and $h = 15.885$. The resulting worst-case scheduling trajectory is shown in Fig. 2. Note that this lower bound is significantly larger than $\gamma_{lb,sin} = 2.5862$ that we obtained in [9] by optimizing over sinusoidal scheduling trajectories. This lower bound coupled with the the dissipation inequality result yields tight bounds on the norm of G: $2.8362 = \gamma_{lb} \leq \|G\| \leq \gamma_{ub} = 2.9640$. Finally, Algorithm 1 was used to construct the worst case input for the worst-case scheduling trajectory. The monodromy matrix $\tilde{Q}$ has a unit modulus eigenvalue at $[-0.9998 + 0.0190i]$. The parameter K in Algorithm 1 was chosen to be $K = 60$. The resulting input is shown in Fig. 2.

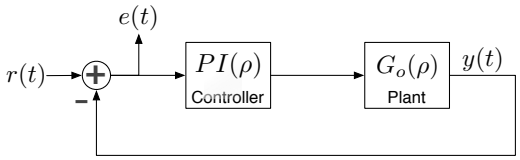

Figure 1. The closed loop interconnection of the parameter-varying plant and the gain-scheduled PI controller in the example presented in Sec. 4.1.

4.2. *Input and output scaled LTI system*

The next example was constructed by taking two copies of the simple LTI system $1/(s+1)$, scaling the input of the first and he output of the second by the same time varying parameter and computing the difference of the two outputs (see Fig. 3). The dynamics of the LPV system obtained are as follows:

$$\begin{bmatrix} \dot{x}_1 \\ \dot{x}_2 \end{bmatrix} = \begin{bmatrix} -1 & 0 \\ 0 & -1 \end{bmatrix} \begin{bmatrix} x_1 \\ x_2 \end{bmatrix} + \begin{bmatrix} 1 \\ \rho \end{bmatrix} w$$
$$z = \begin{bmatrix} \rho & -1 \end{bmatrix} \begin{bmatrix} x_1 \\ x_2 \end{bmatrix}. \tag{30}$$

We assume that $\rho \in [-1\ \ 1]$ and $\dot{\rho} \in [-\overline{\mu}\ \ \overline{\mu}]$. We are going to compute the lower bound for different values of $\overline{\mu}$. It follows from the structure of the system that if ρ is constant then the difference between the input and the output scaled systems is 0. This implies that $\gamma_{lb,fr} = 0$. Next, the upper bound on the $\mathcal{L}_2$ gain was computed for different rate bounds. In all cases the storage function $V(x,\rho)$ and the parameter grid Γ was chosen as follows:

$$V(x,\rho) = x^T \left(P_0 + \sum_{k=1}^{10} \rho^k P_k \right) x$$
$$\Gamma = \{\rho_1 = -1, \ldots, \rho_{100} = 1\},\ \ \rho_{k+1} - \rho_k = 2/99. \tag{31}$$

DOI: 10.1002/rnc

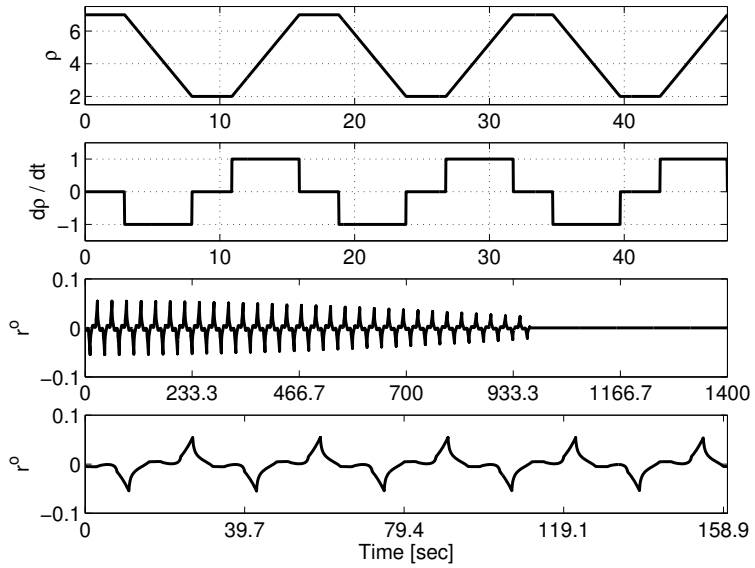

Figure 2. Rows 1 and 2 show the worst case scheduling trajectory and rate for the example in Sec. 4.1. Rows 3 and 4 show the worst-case input over $[0, 1400]$ and zoomed to $[0, 10h]$.

The upper bounds obtained are collected in Table I. The lower bounds, the period of the worst-case scheduling trajectories obtained for the different $\overline{\mu}$ values and the number N of the break points used in the trajectory construction are also given in Table I. The lower bounds $\gamma_{lb,sin}$ we obtained in [9] by using sinusoidal scheduling trajectories are also presented in Table I. It can be seen that by using piecewise linear scheduling signals the lower bounds are significantly larger than those we obtained earlier. Now the upper and lower bounds almost coincide, which means that by using the upper and lower bound algorithms we could precisely compute the norm of this LPV system. The computation time in each case was between 200 and 300 sec. For two particular cases, $\overline{\mu} = 1$ and $\overline{\mu} = 2$, we plotted also the worst case scheduling trajectory and the worst-case input in Fig. 4 and Fig. 5, respectively. (The worst case inputs were computed starting from the unit modulus eigenvalues $[-0.1011 + 0.9949i]$ (in case $\overline{\mu} = 1$) and $[0.9504 + 0.3111i]$ (in case $\overline{\mu} = 2$). K was 60 in both cases.)

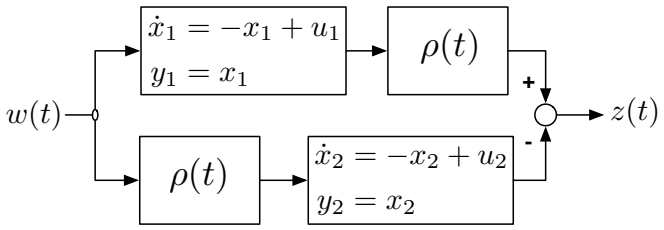

Figure 3. The structure of the LPV system defined in Section 4.2

4.3. A 2-parameter system

The next, more complex example was constructed from the examples in sections 4.1 and 4.2. We took two copies of the closed loop system (28) with scheduling parameter $\rho(t) := \rho_1(t)$, then we scaled the input of the first and the output of the second system by the same time-varying parameter $\rho_2(t)$ and defined the output as the difference between the outputs the two subsystems (like in

DOI: 10.1002/rnc

$\overline{\mu}$	$\gamma_{lb,sin}$	γ_{lb}	γ_{ub}	$\gamma_{ub} - \gamma_{lb}$	h	N
0.1000	0.0825	0.0932	0.1087	0.0155	20	8
0.4000	0.3174	0.3310	0.3342	0.0032	20	8
0.7000	0.4567	0.4764	0.4805	0.0041	9	6
1.0000	0.5448	0.5737	0.5766	0.0029	9	6
1.3000	0.6143	0.6335	0.6435	0.0100	6	6
1.6000	0.6386	0.6861	0.6924	0.0063	6	6
2.0000	0.6893	0.7359	0.7403	0.0044	6	6

Table I. Upper and lower bounds on the $\mathcal{L}_2$ norm of the LPV system defined in Section 4.2

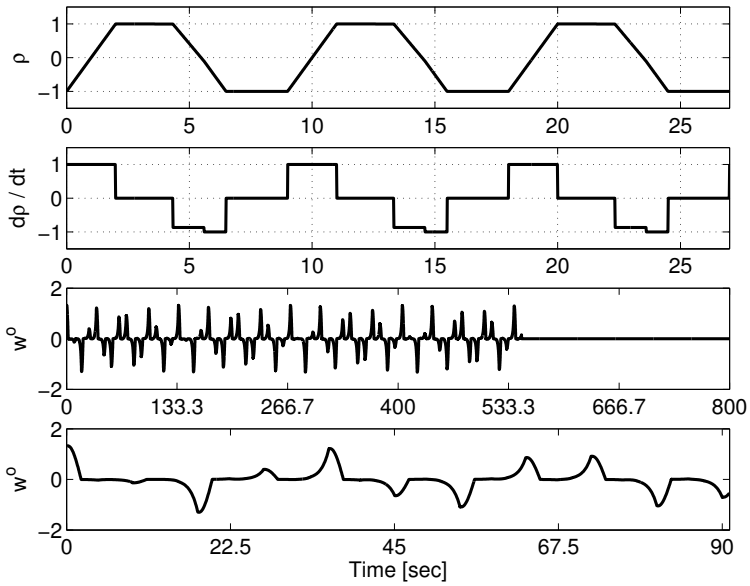

Figure 4. Rows 1 and 2 show the worst case scheduling trajectory and rate for the example in Sec. 4.2 if $\overline{\mu} = 1$. Rows 3 and 4 show the worst-case input over $[0, 800]$ and zoomed to $[0, 10h]$.

Section 4.2). The state-space equations of the system obtained can be written as

$$\begin{aligned} \begin{bmatrix} \dot{x}_1 \\ \dot{x}_2 \end{bmatrix} &= \begin{bmatrix} A(\rho_1) & 0 \\ 0 & A(\rho_1) \end{bmatrix} \begin{bmatrix} x_1 \\ x_2 \end{bmatrix} + \begin{bmatrix} B(\rho_1) \\ \rho_2 B(\rho_1) \end{bmatrix} w \\ z &= \begin{bmatrix} \rho_2 C(\rho_1) & -C(\rho_1) \end{bmatrix} \begin{bmatrix} x_1 \\ x_2 \end{bmatrix}. \end{aligned} \tag{32}$$

The range and rate bounds were as follows: $2 \leq \rho_1 \leq 7$, $-1 \leq \rho_2 \leq 1$ and $-1 \leq \dot{\rho}_1, \dot{\rho}_2 \leq 1$. The construction of the system implies that $\gamma_{lb,fr} = 0$. The upper bound on the induced $\mathcal{L}_2$ norm was computed by using the following storage function and parameter grid:

$$\begin{aligned} V(x,\rho) &= x^T \left(P_0 + \sum_{k=1}^{3} \rho_1^k P_k + \sum_{\ell=1}^{5} \rho_2^\ell P_\ell + \frac{1}{\rho_1} P_9 + \frac{1}{\rho_2} P_{10} \right) x \\ \Gamma &= \{\rho_{1,1} = 2, \ldots, \rho_{1,30} = 7\} \times \\ &\qquad \{\rho_{2,1} = -1, \ldots, \rho_{2,10} = 1\}, \\ &\rho_{k+1,1} - \rho_{k,1} = 2/29, \quad \rho_{\ell+1,2} - \rho_{\ell,2} = 2/9, \\ &k \in \{1 \ldots 30\}, \quad \ell = \{1 \ldots 10\}. \end{aligned} \tag{33}$$

DOI: 10.1002/rnc

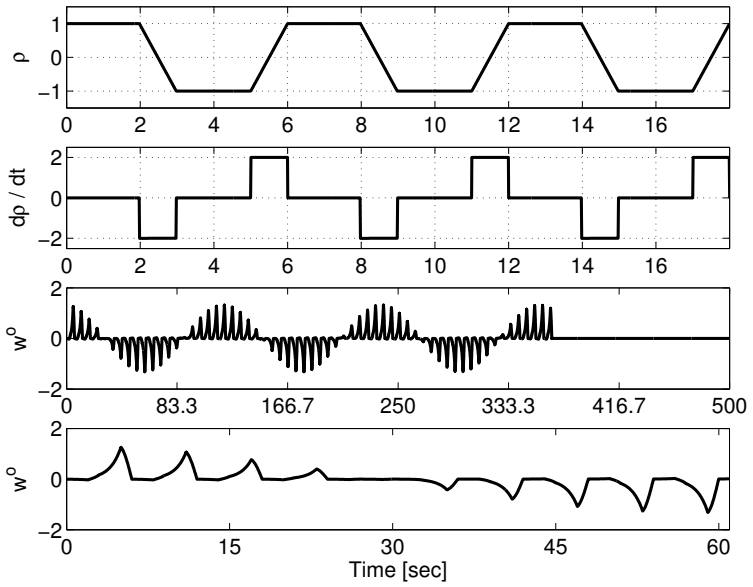

Figure 5. Rows 1 and 2 show the worst case scheduling trajectory and rate for the example in Sec. 4.2 if $\overline{\mu} = 2$. Rows 3 and 4 show the worst-case input over $[0, 500]$ and zoomed to $[0, 10h]$.

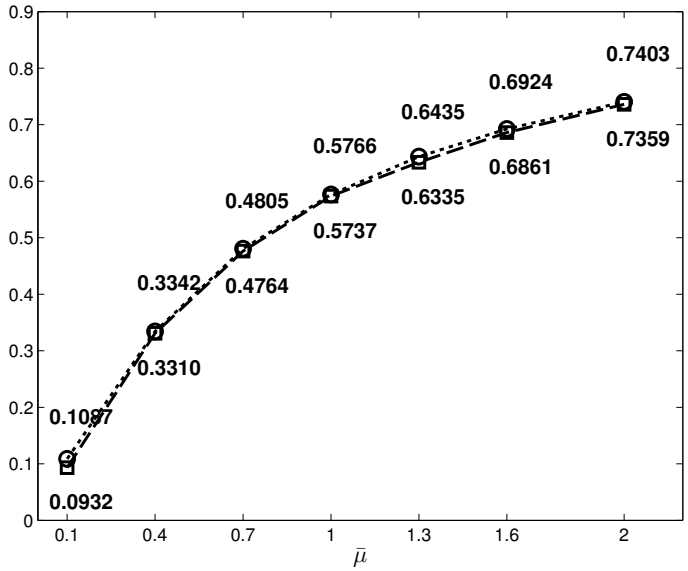

Figure 6. Upper and lower bounds on the induced $\mathcal{L}_2$ norm computed for the example in Section 4.2.

We obtained $\gamma_{ub} = 5.38$. To compute the lower bound we chose $N = 5$ break points for both trajectories. The lower bound we got is $\gamma_{lb} = 5.01$, $(h = 16.18)$, which is again very close to the upper bound. The worst-case scheduling trajectories and the worst-case input are plotted in Fig. 7. (The worst-case input was constructed by starting from the unit modulus eigenvalue $[-0.9997 + 0.0245i]$. The parameter K was set to 60.)

DOI: 10.1002/rnc

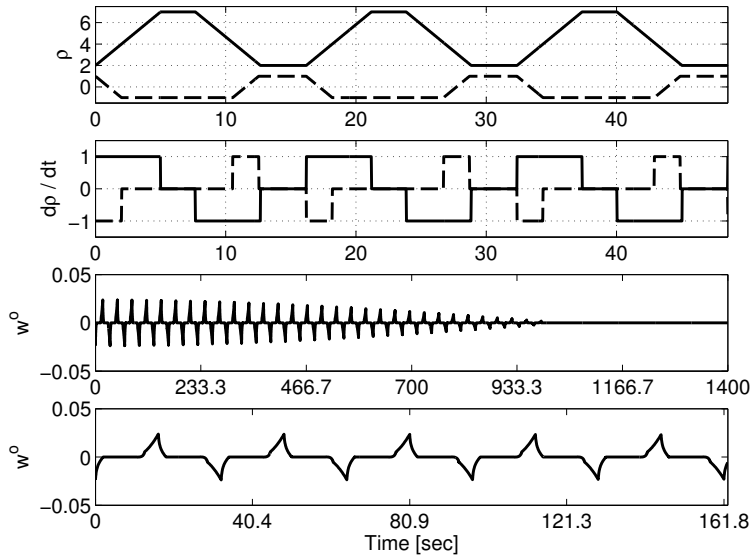

Figure 7. Rows 1 and 2 show the worst case scheduling trajectory and rate for the example in Sec. 4.3. Rows 3 and 4 show the worst-case input over $[0, 1400]$ and zoomed to $[0, 10h]$.

5. CONCLUSION

This paper proposed a numerical method to compute a lower bound on the induced $\mathcal{L}_2$-gain of a continuous-time LPV system. The algorithm finds this bound – together with the worst-case parameter trajectory – by using nonlinear optimization over periodic scheduling parameter trajectories. The restriction to periodic parameter trajectories enables the use of recent results for exact calculation of the $\mathcal{L}_2$ norm for a periodic time varying system. It was shown that the proposed algorithm can be reliably implemented by standard numerical tools and provides precise approximation for the $\mathcal{L}_2$ bound.

A. PROOF OF LEMMA 1

To prove the theorem we need the following properties of the state transition matrix: for all $t, \tau, \tau' \in \mathbb{R}$

(a) $\Phi(t,\tau)\Phi(\tau,t) = I$, which implies $\Phi(t,\tau) = \Phi(\tau,t)^{-1}$

(b) $\frac{d}{dt}\Phi(\tau,t) = -\Phi(\tau,t)A(t)$

(c) $\frac{d}{dt}[\Phi(\tau,t)^*] = -A(t)^*\Phi(\tau,t)^*$.

Item (a) follows from the definition and regularity of $\Phi(t,\tau)$ [8]. Item (b) is a consequence of (a) and can be proved by applying the chain rule to $0 = \frac{d}{dt}\Phi(t,\tau)\Phi(\tau,t)$. Finally, item (c) is the direct consequence of item (b).

The proof of Lemma 1 starts from the definition of the adjoint (Equation (15)):

$$\langle(\hat{x}_h, \hat{z}), \mathbf{T}_G(x_0, w)\rangle = \hat{x}_h^* x(h) + \int_0^h \hat{z}(t)^* z(t)\, dt \tag{34}$$

where $(x(h), z(t))$ are the final state and output of the PLTV system in (1). The solution of (1) can be expressed in terms of the state transition matrix as $z(t) = C(t)x(t)$, where

$$x(t) = \Phi(t,0)x_0 + \int_0^h \Phi(t,\tau)B(\tau)w(\tau)\, d\tau. \tag{35}$$

DOI: 10.1002/rnc

Use this relation to substitute for $x(h)$ and $z(t)$ in Equation (34). Re-arrange terms to obtain the following form:

$$\langle(\hat{x}_h, \hat{z}), \mathbf{T}_G(x_0, w)\rangle = \hat{x}(0)^* x(h) + \int_0^h \left[B^*(\tau)\hat{x}(\tau) + D^*(\tau)\hat{z}(\tau)\right]^* w(\tau)\, d\tau \tag{36}$$

where we have defined the signal

$$\hat{x}(\tau) := \Phi(h,\tau)^*\hat{x}_h + \int_\tau^h \Phi(t,\tau)^* C(t)^* \hat{z}(t)\, dt. \tag{37}$$

Using property (c) above, we obtain

$$\frac{d\hat{x}(\tau)}{d\tau} = -A^*(\tau)\hat{x}(\tau) - C^*(\tau)\hat{z}(\tau), \;\; \hat{x}(h) = \hat{x}_h. \tag{38}$$

If we also define $\hat{w}(\tau) = B^*(\tau)\hat{x}(\tau) + D^*(\tau)\hat{z}(\tau)$, and $\hat{x}_0 = \hat{x}(0)$ then we can express the inner product $\langle(\hat{x}_h, \hat{z}), \mathbf{T}_G(x_0, w)\rangle$ as

$$\hat{x}_0^* x_0 + \int_0^h \hat{w}(\tau)^* w(\tau) d\tau = \langle \mathbf{T}_G^*(\hat{x}_h, \hat{z}), (x_0, w)\rangle. \tag{39}$$

Thus the proof is complete.

ACKNOWLEDGMENT

This work was supported by the NSF under Grant No. NSF-CMMI-1254129 entitled "CAREER: Probabilistic Tools for High Reliability Monitoring and Control of Wind Farms". Any opinions, findings, and conclusions or recommendations expressed in this material are those of the author and do not necessarily reflect the views of the NSF.

The authors greatly acknowledge the help of Henrik Sandberg for making the MATLAB code of the numerical example presented in [6] available for the purpose of this research.

Also, the authors thank the anonymous reviewers for the valuable advices and comments, which have contributed to the improvement of the initial submission.

REFERENCES

1. Apkarian P, Gahinet P. A convex characterization of gain-scheduled $\mathcal{H}_\infty$ controllers. *IEEE Transactions on Automatic Control* 1995; **40**(5):853–864.
2. Scherer CW. LPV control and full block multipliers. *Automatica* 2001; :361–375.
3. Wu F, Yang XH, Packard A, Becker G. Induced $\mathcal{L}_2$ norm control for LPV systems with bounded parameter variation rates. *International Journal of Robust and Nonlinear Control* 1996; **6**(983-998).
4. Wu F. Control of linear parameter varying systems. PhD Thesis, University of California at Berkeley 1995.
5. Rugh WJ, Shamma JS. Research on gain scheduling. *Automatica* 2000; **36**:1401–1425.
6. Cantoni M, Sandberg H. Computing the $\mathcal{L}_2$ gain for linear periodic continuous-time systems. *Automatica* 2009; **45**:783–789.
7. Colaneri P. Continuous-time periodic systems in $\mathcal{H}_2$ and $\mathcal{H}_\infty$: Part i: Theoretical aspects. *Kybernetica* 2000; **36**:211–242.
8. Bittanti S, Colaneri P. *Periodic Systems*. Communications and Control Engineering, Springer, 2009.
9. Peni T, Seiler P. Computation of a lower bound for the induced $\mathcal{L}_2$ norm of parameter varying systems. *Submitted to the American Control Conference (ACC)*, 2015.
10. Bamieh BA, Pearson JB. A general framework for linear periodic systems with applications to $\mathcal{H}_\infty$ sampled-data control. *IEEE Transactions on Automatic Control* 1992; **37**(4):418–435.
11. Bamieh BA, Pearson JB, Francis BA, Tannenbaum A. A lifting technique for linear periodic systems with applications to sampled-data control. *Systems & Control Letters* 1991; **17**:79–88.
12. Zhou K, Doyle JC, Glover K. *Robust and optimal control*. Prentice-Hall, 1995.
13. Dullerud GE, Lall S. Asynchronous hybrid systems with jumps - Analysis and synthesis methods. *Systems & Control Letters* 1999; **37**(61-69).
14. Neishtadt A. *Lectures on Dynamical Systems, Part 1*. Loughborough University 2007. URL http://www.iki.rssi.ru/seminar/virtual/an_part1.pdf.

DOI: 10.1002/rnc

15. Wu F. A generalized LPV system analysis and control synthesis framework. *International Journal of Control* 2001; **74**(7):745–759.
16. MATLAB and Global Optimization Toolbox, Release 2014a. The MathWorks, Inc., Natick, Massachusetts, United States.
17. Pfifer H, Seiler P. Robustness analysis of linear parameter varying systems using integral quadratic constraints. *Accepted to the International Journal of Robust and Nonlinear Control* 2014; .

DOI: 10.1002/rnc